Perturbed angular correlation study of the thiospinel β-In_2S_3

L. Aldon
Laboratoire de Physico-Chimie des Materiaux Solides, Universit de Montpellier 2, 34095 Montpellier Cedex 5, France

M. Uhrmacher
II. Physikalisches Institut, Universität Göttingen, Bunsenstrasse 7/9, D-37073 Göttingen, Germany

C. Branci
Laboratoire de Physico-Chimie des Materiaux Solides, Universit de Montpellier 2, 34095 Montpellier Cedex 5, France

L. Ziegeler, J. Roth, P. Schaaf, and H. Metzner
II. Physikalisches Institut, Universität Göttingen, Bunsenstrasse 7/9, D-37073 Göttingen, Germany

J. Olivier-Fourcade and J. C. Jumas
Laboratoire de Physico-Chimie des Materiaux Solides, Universit de Montpellier 2, 34095 Montpellier Cedex 5, France
(Received 1 April 1998)

The electric field gradients (EFG's) of ^{111}In(EC)^{111}Cd nuclei at the different crystalline sites in spinel β-In_2S_3 have been measured, using perturbed angular correlation spectroscopy. The radioactive ^{111}In tracers were introduced into the samples by means of ion implantation or during the chemical synthesis using natural indium doped with ^{111}In. The radiation damage after the implantation was annealed by heating the samples to above the transition temperature $T=693$ K where the phase transition to cubic α-In_2S_3 occurs. In contrast to previous PAC measurements, three electric field gradients were found. Their temperature dependences were measured in the temperature range between 8 and 743 K. The crystalline structure was checked by x-ray diffraction and refined by means of a Rietveld analysis. Fully consistent with the refined structure, the three observed EFG's were attributed to probes residing in the different sulphur octahedra and tetrahedra of β-In_2S_3. The EFG values are reproduced by the point charge model. A strong damping of the perturbation functions was observed in the temperature range between 150 and 370 K, which was attributed to dynamical hyperfine interactions caused by aftereffects of the electron capture decay of ^{111}In. [S0163-1829(98)05341-7]

I. INTRODUCTION

The perturbed $\gamma\gamma$-angular correlation method (PAC) has often been used as a tool to study, via the hyperfine interaction of a radioactive probe nucleus, the properties of solids such as magnetic and structural phase transitions, chemical reactions, and defects on an atomic scale. Measuring the electric field gradient (EFG) in semiconductors offers the possibility to change the electron density by adding electrically active impurities (e.g., Li) or by varying the temperature. The EFG's at ^{111}Cd probe nuclei on substitutional cation sites for binary metal oxides have been studied systematically in Göttingen,[1–5] including bixbyites (M_2O_3) (Ref. 6) and ternary oxides with either $M_2Cu_2O_5$ structure[7] or delafossite (ABO_2) structure.[8] The PAC experiments for the last three classes of compounds gave information on the local oxygen configuration in terms of the cation size. In all of these compounds the ^{111}In(EC)^{111}Cd probe was found to replace the central cation of the oxygen octahedra.

The structure of the spinels generally is of great interest as it provides the possibility to use the free space in this lattice for storage of foreign atoms such as lithium. Either their exact position, their number, or their chemical binding are of major importance. The large band-gap semiconductor β-In_2S_3 is also interesting as a window material in thin-film $CuInSe_2$ photovoltaic devices.[9]

Spinels are composed of octahedra and tetrahedra. Only a few examples are known where the ^{111}In probe was safely attributed to the central site in an oxygen tetrahedron; in Mn_3O_4 with a high EFG value,[3] in Fe_3O_4,[10] and in $CdIn_2S_4$ (Ref. 11) with a low value. In β-Ga_2O_3, which is also composed of octahedra and tetrahedra, only the octahedral site is occupied by the probe atom.[12] In_2S_3 exists in three phases.[13,14] In the defective spinel β-In_2S_3 (stable up to 693 K), the regular sites of indium atoms are the centers of both disturbed sulphur-octahedra and tetrahedra. In addition, the probe atom does not represent an impurity but belongs to the constituting elements of the compound. Therefore, this compound offers the unique possibility to observe the different types of local environments (octahedra and tetrahedra) under otherwise identical conditions. Furthermore, it will be interesting to find out if the general rules found for oxides will hold for chalcogenes, too.

II. SYNTHESIS OF β-In_2S_3

All the samples were prepared by solid state reactions. The binary thiospinel β-In_2S_3 was synthesized by means of a direct reaction from stoichiometric mixtures of the elements in evacuated tubes ($P=10^{-3}$ Pa). Afterwards, this mixture was heated up to 573 K for one day. Then, the temperature was raised to finally reach a value of 1373 K which remained

constant for three hours. As an annealing treatment, the temperature was then kept at 1073 K for eight days. Pellets made from each substance were implanted with $^{111}In^{+}$ ions at an energy of 400 keV and a total dose of about 10^{12} ions, using the Göttingen ion implanter IONAS.[15,16] Then the samples were annealed under the conditions described below in order to remove the radiation damage.

One sample was synthesized using indium metal, into which the radioactive ^{111}In tracer atoms were introduced by electrolysis. The deposition of ^{111}In was performed in an electrochemical cell with a natural indium cathode and a platinum anode. The electrolyte was a mixture of Na_2SO_4, an ammonium salt, and $^{111}InCl_3;6H_2O$. A voltage of 5 V was applied to the cell loading to a current of 140 mA. Finally, the electrochemical reaction was

$$\begin{aligned} \text{cathode:}\quad & {}^{111}In^{3+}+3e^{-}\rightarrow {}^{111}In^{0}, \\ & 2H^{+}+2e^{-}\rightarrow H_2, \\ \text{anode:}\quad & 4OH^{-}\rightarrow O_2+4e^{-}+2H_2O. \end{aligned} \tag{1}$$

After the electrolysis, 0.41955 g of indium, containing an activity of 0.41 mCurie of ^{111}In tracers, were placed in a tube together with the sulphur, to react to β-In_2S_3. Subsequently, the same thermic program was performed as in the case of the nondoped samples.

III. PAC METHOD AND APPARATUS

The time-differential perturbed angular correlation technique with radioactive ^{111}In probe atoms was used to measure the EFG's at the different crystallographic sites of β-In_2S_3. A detailed description of this method can be found in the literature.[17–19] The short overview given here will demonstrate how, in principle, the EFG in a solid compound can be measured.

The EFG is a tensor V_{ij} defined by the second derivative of the electric potential $V(r)$ at the probe site. Its nine components can be reduced to the three diagonal elements V_{xx}, V_{yy}, and V_{zz}, arranged as $V_{xx}\leqslant V_{yy}\leqslant V_{zz}$. The diagonal traceless tensor is completely described by the largest of the three components (V_{zz}) and the asymmetry parameter $\eta=(V_{xx}-V_{yy})/V_{zz}$ with $0\leqslant\eta\leqslant 1$. The quadrupole interaction coupling constant $\nu_Q=eQV_{zz}/h$ represents the strength of the EFG and η is a measure of the tensor's deviation from axial symmetry ($V_{xx}=V_{yy}$).

The probe atom ^{111}In decays with a half-life of $T_{1/2}=2.83$ days to the excited $7/2^{+}$ state of ^{111}Cd via electron capture (EC). This state, in turn, decays to the $1/2^{+}$ ground state of ^{111}Cd via the emission of the 171–245 keV $\gamma\gamma$ cascade. The intermediate $5/2^{+}$ level is characterized by the quadrupole moment $Q=0.83$ b, the magnetic moment $\mu=-0.766\mu_N$, and the half-life $T_{1/2}=85$ ns.[18]

The perturbed time-differential angular correlation in polycrystalline materials is expressed by

$$W(\theta,t)=1+A_{22}G_{22}(t)P_2(\cos\theta), \tag{2}$$

where θ is the angle between the detectors. A_{22} is the anisotropy coefficient of the $\gamma\gamma$ cascade, $P_2(\cos\theta)$ is the second Legendre polynomial, and $G_{22}(t)$ is the perturbation factor, containing all the information on the hyperfine interaction. In the case of static electric interaction, $G_{22}(t)$ is defined as

$$G_{22}(t)=\sum_{n=0}^{3} S_{2n}(\eta)\cos(\omega_n t) \times\exp[-g_{2n}(\eta)\delta t]d[g_{2n}(\eta)\nu_Q t,\tau_R] \tag{3}$$

with ω_n being the primary transition frequencies and S_{2n} their respective amplitudes; their values are defined in Ref. 20. The parameter δ denotes the width of a Lorentzian distribution of the EFG and the function $d[g_{2n}(\eta)\nu_Q t,\tau_R]$ accounts for the damping of $G_{22}(t)$ due to the finite time resolution τ_R of the apparatus. The PAC experiments were carried out using a conventional slow-fast setup with four NaI(Tl) detectors in 90° geometry or a fast-fast setup[21] with four BaF_2 detectors positioned in the same geometry. Then, the twelve time spectra obtained from all possible combinations of the four detectors were used to calculate the experimental perturbation function $R(t)$, given by

$$R(t)=2\frac{N(180,t)-N(90,t)}{N(180,t)+2N(90,t)}=A_{22}\sum_{i=1}^{5} f_i G_{22}^{i}(t), \tag{4}$$

where f_i denotes the relative fractions for different EFG's contributing to the PAC spectrum and $G_{22}^{i}(t)$ the corresponding perturbation factors.

IV. EXPERIMENTAL RESULTS

A. PAC measurements

PAC measurements in the different phases of In_2S_3 were performed in the 1980's during the investigation of the $T^{3/2}$ scaling behavior of the EFG's in metals and compounds.[22] The most detailed study in this context is Gabriele Lanzendorfer's diploma thesis.[23] She found two nearly axially symmetric EFG's in the temperature range between 25 and 623 K: about 75% of the probes showed an EFG with $\nu_Q=65$ MHz, which did not depend on the measuring temperature T_m. The rest were found to have a temperature-dependent EFG of $\nu_Q=140$–122 MHz. From the known ratio of the number of octahedral/tetrahedral sites in the spinel structure (75/25) she attributed the lower EFG to probes on the octahedral site. At high temperatures ($T_m\geqslant 1048$ K) only one EFG with $\nu_Q=119.5$ MHz was observed in the γ phase of In_2S_3. Following the crystallographic data, at these temperatures only octahedral sites are occupied by In and, consequently, this EFG was attributed to In at the octahedral site in the γ phase of In_2S_3. As the probe ^{111}In is always a host atom of the compound, only substitutional sites have to be considered in well annealed material.

1. Annealing behavior

As already described in Sec. II the synthesis of all the In_2S_3 samples ended with an eight-day annealing at 1073 K as the last step. For the ^{111}In implantations, the powder-material had to be pressed to pellets of 4 mm diameter. After the implantation further annealing in vacuum was necessary to remove the radiation damage introduced by the implantation. Figures 1(a)–1(d) show a series of PAC spectra taken at room temperature (RT) after heating the implanted sample

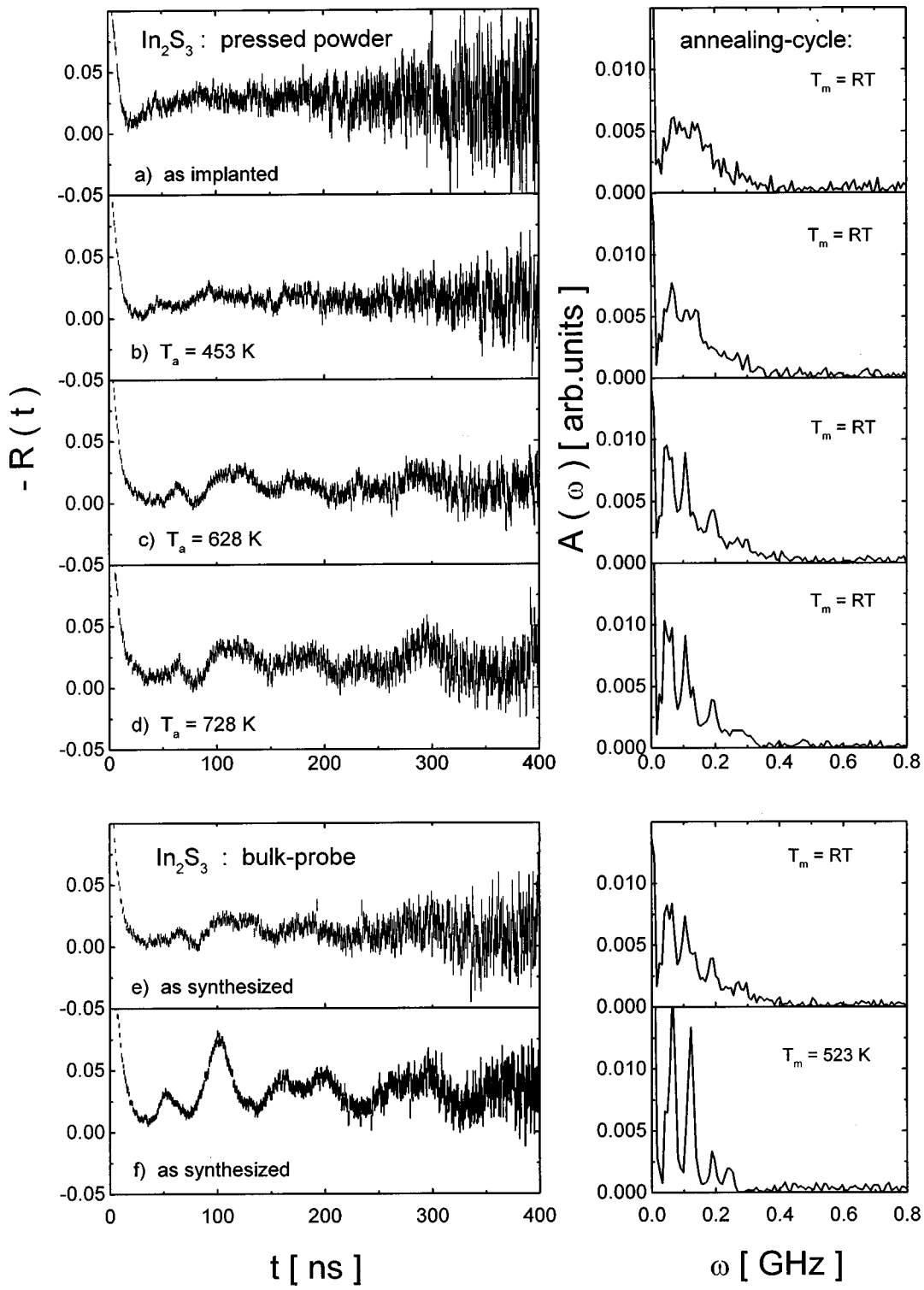

FIG. 1. Annealing behavior of a β-In_2S_3 sample implanted with ^{111}In. The PAC spectra and their Fourier transforms are shown, measured at RT after annealing in vacuum for 1 h at different temperatures T_a (a)–(d). For comparison, PAC spectra from the chemically doped bulk sample are shown obtained at different measuring temperatures T_m (e),(f).

for one hour at increasing annealing temperatures T_a. After allowing for a phase transition into the cubic α phase ($T \geqslant 693$ K), the sample is perfectly annealed. This can be seen by a comparison with Fig. 1(e), taken at RT from the bulk sample which was chemically doped with ^{111}In. There is no obvious difference between the implanted and the chemically doped samples. The small intensity differences in the Fourier spectra observed at higher temperatures [Fig. 1(f)] can be explained by a macroscopic-visible texture of the bulk sample.

2. Temperature dependence of the EFG's

After annealing the radiation damage, the PAC spectra were measured at different temperatures T_m which are indi-

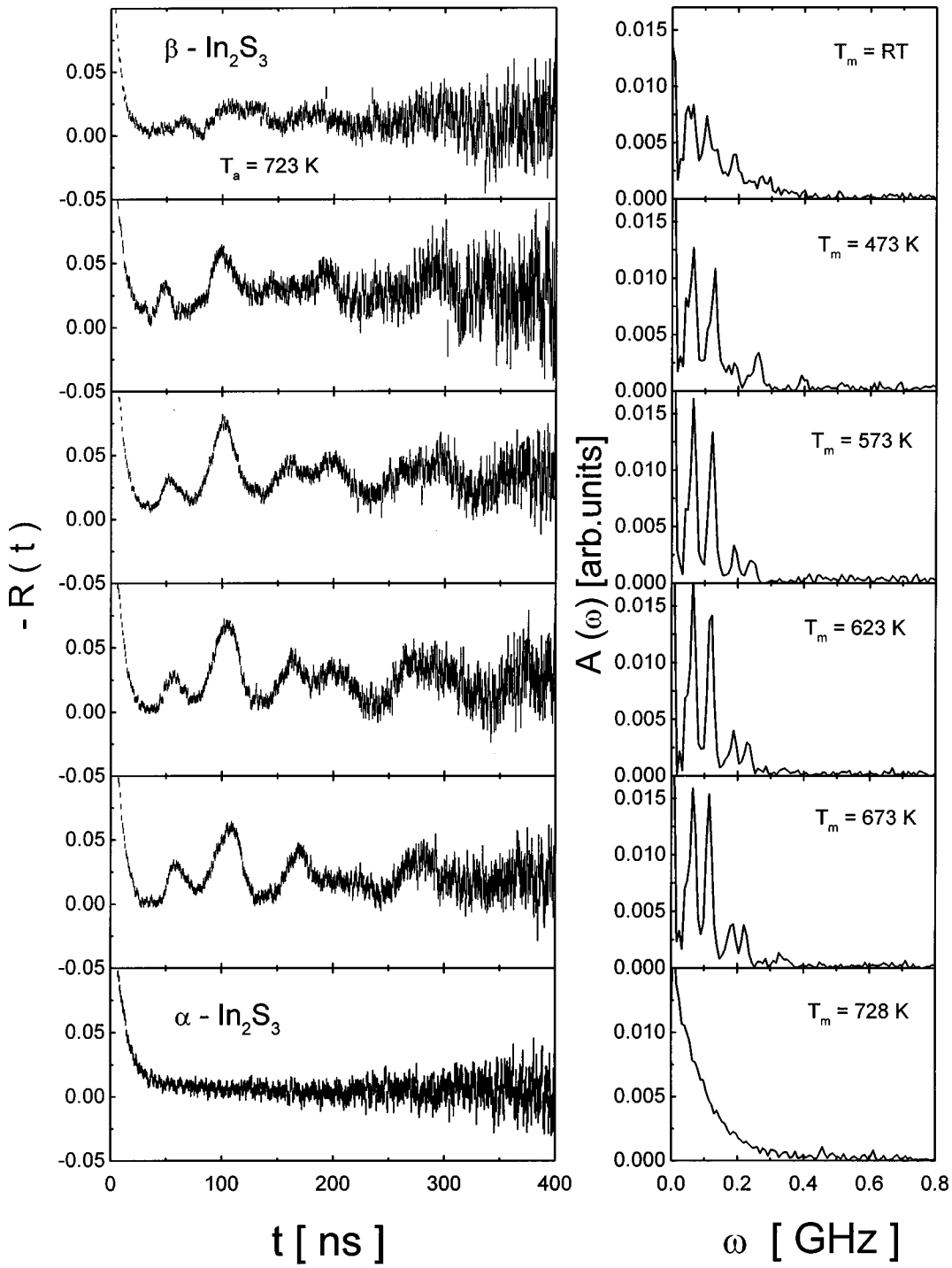

FIG. 2. PAC spectra and their Fourier transforms for ^{111}Cd in annealed β-In_2S_3, measured in vacuum at different measuring temperatures $T_m \geqslant$ RT.

cated in Figs. 2 and 3. The temperatures were chosen in random order. All the PAC spectra had to be fitted with a set of three different frequencies. As the result, two of them (ν_{Q2} and ν_{Q3}) agree quite reasonably with the ones found in the previous PAC experiments.[22,23] The third one is a lower frequency, characterized by the EFG parameters $\nu_{Q1} = 35$ MHz and $\eta_1 = 0.6$. In all the Fourier spectra, the first peak of this triplet is either clearly separated from the larger one at about 60 MHz or at least visible as a shoulder on the left side of the large peak. In fact, the fractions f_1 and f_2 of these two EFG's amount to 75%. This value was fitted in Ref. 23 for the dominant EFG with $\nu_Q = 65$ MHz. It seems that in the measurements of Refs. 22,23, the experimental resolution did not allow one to detect the lowest frequency. Furthermore, the temperature region from 150 to 300 K was not shown or discussed in Refs. 22,23. The low-temperature measurements given in Fig. 3 show a dramatic damping of the perturbation function in that temperature region, whereas at lower temperatures the three frequencies reappear. A similar behavior was observed in some oxides, especially in La_2O_3 (Ref. 24) and also in In_2O_3 (Ref. 25). In these cases, it could be proven by using ^{111m}Cd probes, that the after

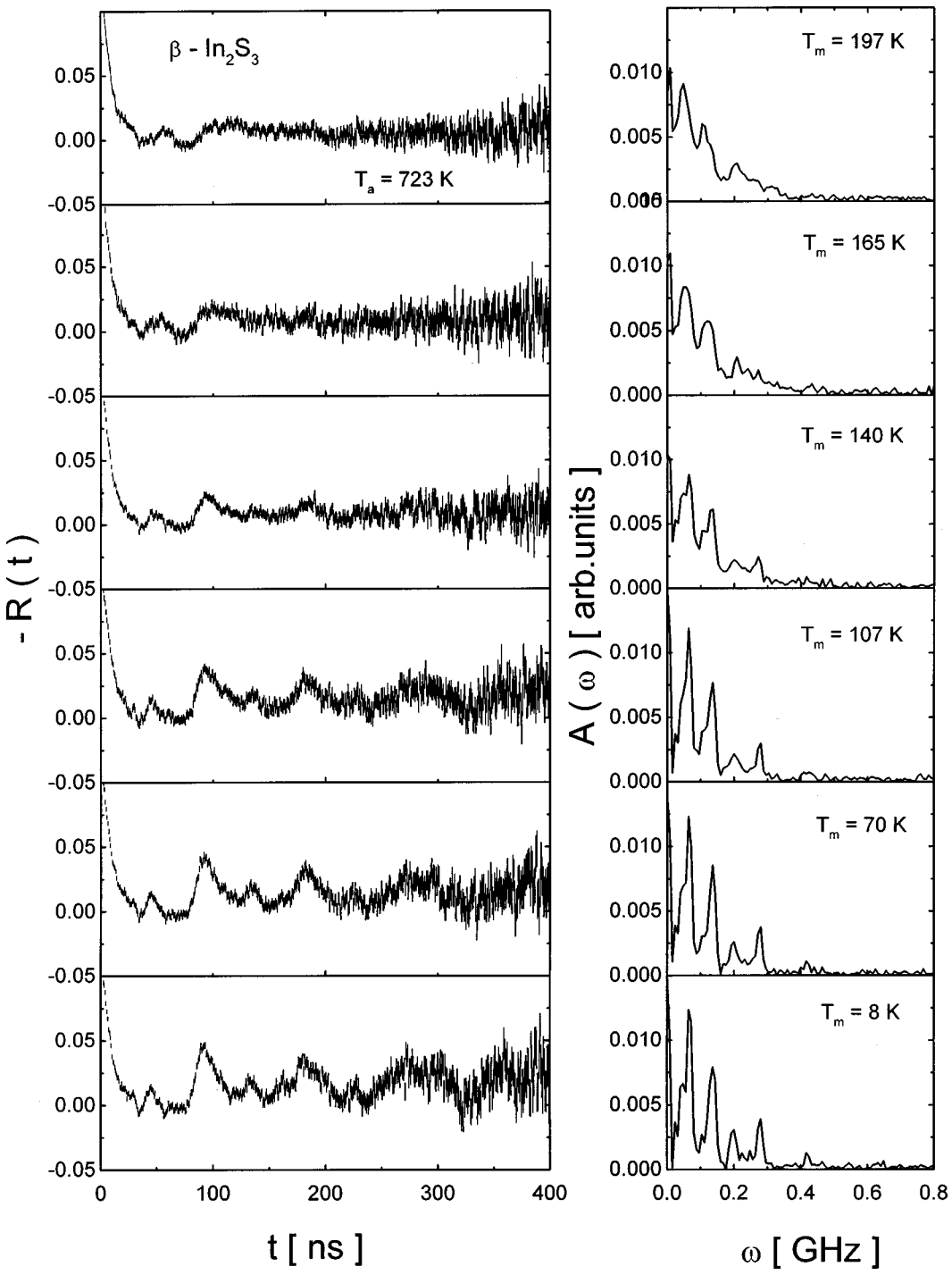

FIG. 3. PAC spectra and their Fourier transforms for ^{111}Cd in annealed β-In_2S_3, measured in vacuum at different measuring temperatures $T_m \leqslant$ RT.

effect of the ^{111}In probe's electron-capture decay causes dynamical hyperfine interactions: damping occurs when in a semiconductor a low availability of electrons leads to relaxation phenomena within the PAC observation time. In these cases[24–26] at very low temperatures the sharp frequencies reappeared which was interpreted as an increased electron availability at the probe, caused by either a change of the conductivity mechanism or the closure of other electron traps. As will be reported in a forthcoming paper,[27] the doping of In_2S_3 with the electron-donor Li suppresses the damping of the $R(t)$ function in this temperature range—a clear proof of our assumption.

The (various) EFG parameters ν_{Qi}, δ_i, and η_i obtained by fitting the spectra of the present work are also summarized in Table I. As the data obtained from implanted samples and chemically doped samples agree with each other, all the temperature-dependent PAC parameters are given together in Fig. 4. In the region of strong damping (between 150 and 370 K), ν_{Qi} and η_i were fixed and the damping was accounted for by fitting an increasing distribution width δ_i.

The last diagram of Fig. 2, taken at $T_m = 728$ K, is one example of a PAC spectrum of the cubic α-In_2S_3 phase characterized by an exponentially decreasing perturbation func-

TABLE I. Experimental hyperfine parameters at different measuring temperatures T_m (K) for β-In_2S_3. ν_{Qi} is the quadrupole coupling constant and δ_i the width of a frequency distribution, both are given in MHz. η_i is the asymmetry parameter and $f_i(\%)$ the observed fraction. Previous data for γ-In_2S_3 are shown in addition.

T_m	ν_{Q1}	η_1	δ_1	f_1	ν_{Q2}	η_2	δ_2	f_2	ν_{Q3}	η_3	δ_3	f_3	Phase
8	39.7	0.46	6.7	39.6	70.1	0	2.6	38.2	147.7	0.14	2.6	22.1	
70	36.6	0.47	9.7	47.2	69.7	0	2.3	32.4	146.9	0.12	2.1	20.4	
87	34.7	0.59	5.8	40.1	70.3	0	4.4	39.0	146.0	0.12	3.7	20.9	
107	35.9	0.52	8.8	35.9	68.8	0	4.7	39.9	145.6	0.10	3.4	19.3	
140	35.9	0.29	9.4	40.0	68.8	0	8.3	35.0	145.6	0	11.5	25.0	
165	35.9	0.29	9.9	40.0	68.8	0	11.1	35.0	145.6	0	20.0	25.0	
293	34.2	0.6	0.0	10.8	63.1	0.12	24.6	76.2	140.0	0.0	16.0	13.0	β
473	35.0	0.52	2.6	21.6	63.4	0.19	7.4	55.9	137.8	0.04	2.0	22.5	
523	36.2	0.5	0.8	22.2	65.0	0.18	2.8	52.2	135.1	0.03	1.6	25.6	
573	37.7	0.5	1.8	21.9	65.0	0.23	4.0	61.5	129.8	0.06	2.6	16.5	
628	39.2	0.5	1.3	23.1	64.4	0.23	3.2	60.2	122.3	0.0	2.1	16.7	
673	38.7	0.5	2.6	26.7	62.2	0.34	3.8	62.2	118.4	0.03	0.9	14.8	
674	37.2	0.59	5.3	32.4	64.1	0.34	1.5	40.7	116.7	0.02	3.9	26.8	
293	34.6	0.59	0.14	25.6	61.9	0.97	22.9	53.9	161.7	0.52	6.7	20.5	
383	35.7	0.60	0.0	24.6	62.7	0.19	21.5	50.6	138.1	0.08	2.6	24.8	β [a]
523	37.6	0.54	0.0	29.3	67.2	0.02	0.2	53.2	133.9	0.03	0.1	17.4	
673	31.5	0.96	5.9	30.5	64.4	0.35	1.7	45.0	116.1	0.01	3.1	24.5	
1048									119.5	0.0	10.1	100	γ
1172									103.1	0.0	4.8	100	(Refs. 22,23)

[a]The bulk sample.

tion. As discussed in Ref. 28, such a spectrum can be fitted assuming a broad ($\delta = 420$ MHz) frequency distribution around a central value of $\nu_Q = 0$, or it can be fitted with an exponential function $\exp(-\lambda t)$ having a decay constant $\lambda = 83$ MHz.

B. XRD measurements

The purity and structure of both types of In_2S_3 samples, either chemically synthesized (powder samples) or prepared with radioactive tracers (bulk sample), were examined by x-ray powder diffraction (XRD) with a Philips θ-2θ diffractometer, using CuK_α radiation and a nickel filter. The Rietveld refinements were carried out with the aid of the computer code DBWS-9006 developed by Wiles and Young.[29]

The Rietveld analysis confirms that no drastic variations occur in the lattices, they do not depend on the compounds preparation method. An XRD spectrum of the sample prepared with radioactive tracers is presented in Fig. 5 and the results are summarized in Table II. They demonstrate that the radioactive synthesis does not involve any change in the compound structure. The structural parameters are in good agreement for both types of compounds (powder and bulk sample). As the main result, it is confirmed that β-In_2S_3 can be described in the $I4_1/amd$ space group with cell parameters a_Q and c_Q of about 7.6 and 32.3 Å, respectively, where $a_Q \approx \sqrt{2/2}\,a_c$ and $c_Q \approx 3a_c$ (a_c is the cell parameter of cubic α-In_2S_3).

The calculated reflections match very well with the x-ray diffraction pattern shown in Fig. 5. We obtained the correlation factors $S = 2.17$ and $R_{\mathrm{Bragg}} = 4.07$ validating our structural hypothesis. Three different In sites were obtained from this analysis. Two of them are located in octahedral sites $8c$ and $16h$, the third one occupies a tetrahedral site $8e$. Furthermore, this analysis shows that the two nonequivalent octahedral sites have important differences in their local environments. Site $8c$ may be described by classical Jahn-Teller compression along the c axis. This site is surrounded by four sulphur atoms placed in a planar square at a distance of 2.68 Å and two additional sulphur atoms at a distance of only 2.54 Å above and below. The situation is completely different for site $16h$. In this case, the two smallest sulphur distances (2.55 Å) make an angle of 90° instead of 180° (Fig. 6). Table II summarizes the results of the parameter refinement.

V. DISCUSSION

The compound In_2S_3 has a model aspect: as a host atom, the PAC probe ^{111}In should occupy all possible cation sites. Therefore, according to the XRD analysis of the structure, we expect to find three different sites for the probe in the β phase of In_2S_3, a tetrahedral site and *two* nonequivalent octahedral sites (see Fig. 6). In fact, the main difference between our present work and the study reported previously[22,23] is the observation of an additional frequency of about 35 MHz. The following section will explain how the three observed EFG's can clearly be attributed to the three sites in the β phase. Due to this a new interpretation of the previous PAC data is required. As a by-product it gives a

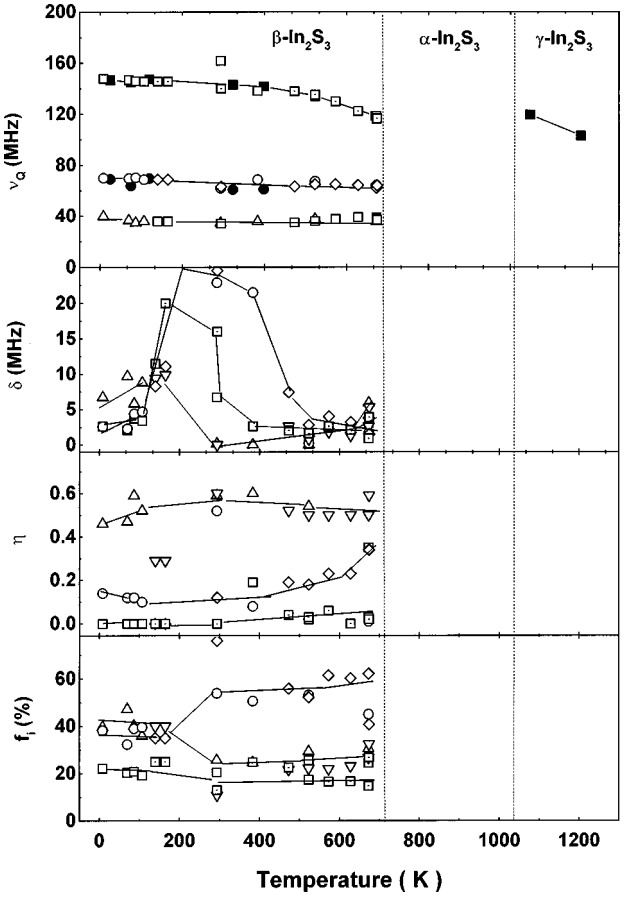

FIG. 4. Temperature dependence of all the fitted PAC parameters for ^{111}Cd in In_2S_3. In the first diagram the results of the previous experiments are given as filled points.

simple explanation of the previous data on the high-temperature γ phase of In_2S_3.

A. Site identification

In the case of β-In_2S_3, the values of the different fractions observed in the PAC spectra can be taken as the strongest indication of a specific site. As shown in Fig. 4, the three frequencies appear above RT with the nearly constant fractions $f_1 \approx 27\%$, $f_2 \approx 53\%$, and $f_3 \approx 20\%$ close to the numbers 25, 50, and 25 % expected from the crystallographic

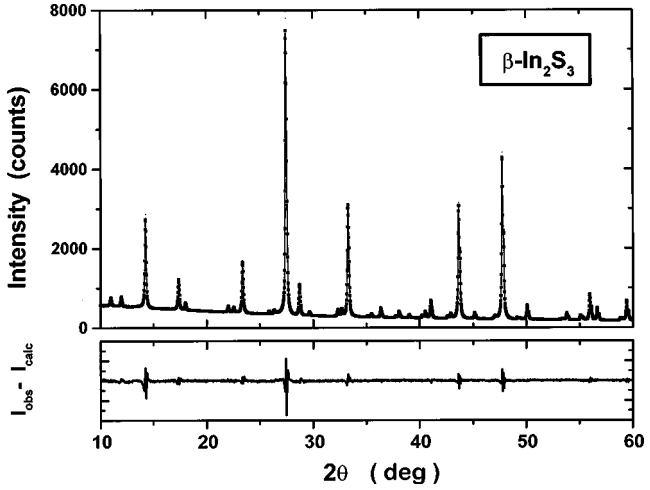

FIG. 5. XRD pattern of the β-In_2S_3 bulk sample, chemically doped with ^{111}In during the synthesis.

analysis. This allows a direct attribution of EFG(2) to probes residing on the distorted octahedral In site 16*h* with the symmetry O_{h2}.

Additional arguments are needed to find out which EFG corresponds to probes at the tetragonal site, as both remaining fractions are about equal. Here we use first the experimental results known for γ-In_2S_3. This high-temperature modification of In_2S_3 has a layered trigonal structure, in which only octahedral sites are occupied by In atoms.[14] Consequently, this leads to only one frequency in the PAC spectra, which has been reported previously by Frank *et al.*[22] As given in Table I, the observed frequency at 1048 K is $\nu_Q = 119.5$ MHz, surprisingly close to the value $\nu_{Q3} = 118.4$ MHz which was observed at the highest temperatures in the β phase (673 K). Therefore, we propose that EFG(3) corresponds to the symmetric octahedral site 8*c* with the symmetry O_{h1}.

This site allocation simply eliminates the dilemma of Refs. 22,23: as these authors missed EFG(1) due to their experimental resolution, they had to attribute EFG(3) to the tetrahedral site, using the general ratio between the number of octahedral and tetrahedral sites in the spinel structure. As a result, the EFG on a tetrahedral site in the β phase seemed to be identical to the one on the octahedral site in the γ

TABLE II. Structural parameters obtained from the Rietveld analysis of the x-ray diffraction pattern for the three different In sites in β-In_2S_3. Two parameters (S and R_{Bragg}) control the refinement. R_{Bragg} characterizes the difference between the theoretical and experimental intensities of the Bragg reflections. S is a similar parameter, which takes into account the complete XRD pattern.

In_2S_3	Position	x/a	y/b	z/c
In(T_d)	(8*e*)	0	0.2500	0.2042(2)
In(O_{h1})	(8*c*)	0	0	0
In(O_{h2})	(16*h*)	0	0.0247(8)	0.3329(2)
S	(16*h*)	0	0.0020(28)	0.2514(4)
S	(16*h*)	0	0.0042(31)	0.0806(4)
S	(16*h*)	0	0.0018(28)	0.4162(5)
$I4_1/amd$	$a = 7.6143(3)$	$c = 32.3078(13)$	$R_{\mathrm{Bragg}} = 4.07$	$S = 2.17$

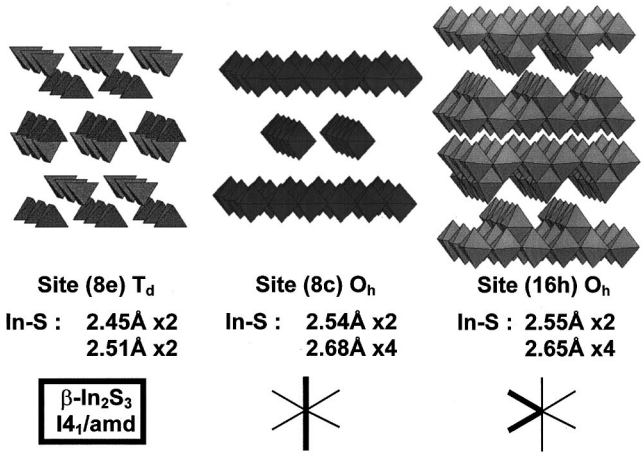

FIG. 6. Crystalline structure of β-In_2S_3. The three different In neighborhoods (note the zig-zagging of the octahedra baseline only for site 16*h*) are shown. The In-*S* distances are given and the directions of the shorter bondlength.

phase. Using our new interpretation, EFG(3) always corresponds to probes in the center of a symmetric sulphur octahedron.

Our identification of EFG(1) as the tetrahedral site is also supported by the results of Mössbauer experiments (MS). The spinel In_2S_3, in which one third of the tetrahedral cation sites are unoccupied, can be used as a host lattice for solid solutions within the system In_2S_3-FeS. Up to 55 mol % of FeS can be solved in In_2S_3.[30] All such solid solutions show the spinel structure of α-In_2S_3. If ^{57}Fe is introduced as a local probe, the structural vacancies of the spinel structure can be detected by means of Mössbauer spectroscopy.[31,32] Several typical values of quadrupole splittings have been observed which can be related to the number of vacant tetrahedral sites around an iron atom. In the case of α-In_2S_3, the main contribution to the quadrupole splitting of about 3.16 mm/s (Refs. 31,32) comes from a trigonal distortion of the sulphur octahedron.[33] A small contribution of about 0.77 mm/s was attributed to Fe on tetrahedral sites, mainly by comparing to the MS parameters found in many other iron-sulphur spinels.[34]

In order to compare the hyperfine parameters from Mössbauer spectroscopy (quadrupole splitting) and the PAC technique (quadrupole coupling constant Δ) we can calculate the ratio $\Delta_O/\Delta_T = 3.16/0.77 = 4.1$ from the MS results. This ratio, in turn, can be directly compared to the ratio of the frequencies (taken at 473 K) $\nu_{Q3}/\nu_{Q1} = 137.8/35 = 3.9$. Our site attribution is confirmed by this good agreement.

B. Point charge model calculations

It is known[35] that in ionic oxides the PCM reproduces the coupling constants and asymmetry parameters quite well as long as the distances between the probe and its nearest neighbors are larger than 2.1 Å. Although in sulphides such a rule has not been shown yet, we may apply a similar scaling and expect a critical distance of 2.54 Å (the sum ionic radii of S^{2-} and In^{3+} ions). In In_2S_3, most of the distances at the three different cation sites are larger and the PCM may be applied, using the standard antishielding factor $\gamma_\infty = -29.27$.[36,37] The results obtained by PCM calculations are reported in Table III and compared to the experimental results.

The strength of all three EFG's is quite well reproduced by the PCM calculations. This can be taken as a further confirmation of our site identification. On the other hand, the predictions of the asymmetry parameters η_2 and η_3 are quite wrong. Figure 4 shows that at most temperatures η_2 is about 0.2 and finally rises to the value of 0.35, close to the $\beta \rightarrow \alpha$ phase transition. But η_3 is always close to zero, different from the PCM calculation. This points to a serious problem, as the asymmetry parameter is safely predicted by the PCM—at least in the oxides. An explanation may be found in the fact that the binding in the thiospinel In_2S_3 already has a more covalent character. The uncertainty where to localize the charges makes the PCM less successful in the case of covalent binding. This different type of binding might also explain why indium ions can be found in a site of tetrahedral symmetry in this structure.

C. Temperature dependences

The temperature dependence of the PAC parameters is given in Fig. 4. To account for the strong damping of the perturbation functions in the temperature range between 150 and 370 K, the width δ_i was allowed to strongly increase while the other parameters were fixed. As already mentioned above, we propose that the strong damping occurs due to dynamic hyperfine interactions following the EC decay of ^{111}In. Such a strong damping was not reported before and $R(t)$ functions from this temperature range are not shown in Refs. 22,23. The temperature dependences of ν_{Q2} and ν_{Q3} are in perfect agreement with the data of Refs. 22,23. Com-

TABLE III. PCM calculation for the three different sites in β-In_2S_3 and in α-In_2S_3. For comparison, the experimental values of the ^{57}Fe Mössbauer quadrupole splitting Δ for the octahedral and tetrahedral sites in α-In_2S_3 are given, as well as the ^{111}In quadrupole coupling constants ν_{Qi} (MHz); the asymmetry parameters η_i obtained in this work are given for the spectra recorded at 473 K.

In_2S_3	site	$(1-\gamma_\infty)\nu_Q$(pcm)	η(pcm)	Δ_{exp}(mm/s)	ν_Q^{exp}	η^{exp}
α	25% T_d	35.2	0.35	0.77		
	75% O_h	144.2	0.03	3.16		
β	25% T_d	31.2	0.34		35.0	0.52
	25% O_{h1}	170.5	0.86		137.8	0.04
	50% O_{h2}	74.5	0.54		63.4	0.19

paring the behavior of the two different sulphur octahedra, we find that EFG(3) of the symmetrical octahedron decreases with temperature without changing the asymmetry parameter. In a purely ionic picture, this simply tells that the size of the octahedron increases. EFG(2) of the asymmetric octahedron stays constant, but its symmetry changes in the vicinity of the phase transition $\beta \rightarrow \alpha$. The PAC parameters for the tetrahedral site seem to be temperature independent, which can be understood as the sign for the stability of the sulphur tetrahedron in the β phase of In_2S_3.

The XRD pattern of β-In_2S_3 is characteristic of the quadratic distortion of the cubic structure of α-In_2S_3. Therefore, the structure analysis of the lattice specifies three sites for the In atoms in the ratio 8:16:8 (T_d,O_{h2},O_{h1}). During the $\beta \rightarrow \alpha$ transformation the two different octahedral sites 8*c* and 16*c* are involved in a global translation of their centers, leading to a single octahedral site 16*d* of cubic structure (space group $Fd3m$). This mechanism corresponds to an order/disorder transition of the distribution of empty sulfur tetrahedra. As described above, both octahedra change their parameters (O_{h1} the frequency and O_{h2} the asymmetry) with increasing temperature, which may already be the beginning of the $\beta \rightarrow \alpha$ transformation of the lattice.

Finally, the temperature behavior of the different site population has to be discussed. At temperatures above 300 K, the measured fractions are in agreement with the results of the XRD analysis, but below 200 K a change may be deduced from Fig. 4: f_1 and f_2 are both found with 40%. This might be the indication of a different crystalline phase at low temperatures. On the other hand, the observed change in the two fractions may be artificial, caused by the difficulties in the fitting procedure. As the first peaks of both frequency tripels of the two EFG's partially overlap, their intensities are less safe to determine in case of an increasing frequency distribution width. Only with the help of a low-temperature XRD measurement can the question of the existence of a new low-temperature phase be answered.

VI. CONCLUSIONS

The β phase of In_2S_3 has a defective spinel structure, where a fraction of the sulphur tetrahedra is empty, i.e., no In ion is found in the center. The $\beta \rightarrow \alpha$ transition of the lattice at 693 K corresponds to an order/disorder transition of the distribution of empty sulfur tetrahedra. Before studying the possible use of this free space to insert foreign ions, the existing microsurroundings for cations in this structure have to be well understood.

The compound In_2S_3 has model character: as a host atom the PAC probe ^{111}In occupies all the possible cation sites. In fact, the main difference between our present work and the previous studies is the observation of an additional EFG(1) having a frequency of about 35 MHz. In agreement with the refinement of XRD spectra taken from the same samples, here we identified three different sites for the ^{111}In probe in the β phase of In_2S_3, a tetrahedral site and especially two *nonequivalent* octahedral sites. This identification leads to an interpretation of the previously reported EFG(2) and EFG(3), which are now attributed to the two different octahedral sites. As a consequence, we now obtain agreement with two other experiments: in the γ phase of In_2S_3, only octahedral sites are occupied by In at high temperatures and only one EFG with $\nu_Q = 119.5$ MHz was observed.[22,23] Its parameters agree surprisingly well with EFG(3) now attributed to one of the octahedral sites. Furthermore, Mössbauer spectroscopy with FeS-doped In_2S_3 gives the ratio of EFG's at the octahedral/tetrahedral site with 4.1, which is in good agreement with the frequency ratio $\nu_{Q3}/\nu_{Q1} = 137.8/35 = 3.9$.

The experimental EFG's can be reproduced by the PCM but, in contrast to the case of oxides, the asymmetry parameters are not predicted correctly. A possible explanation can be found in the different type of binding. In most cases oxides show highly pure ionic binding. As a consequence, the ^{111}In probe is usually found in the center of oxygen octahedra. In In_2S_3, covalent binding appears and the ^{111}In probes can be found in sulphur tetrahedra, too. Therefore, one has to expect less good agreement of PCM predictions in sulphides.

Both types of octahedra change their parameters above 400 K with increasing temperature which may already be the beginning of the $\beta \rightarrow \alpha$ transition of the lattice. A change of the fractions at low temperatures may be interpreted as an indication of a still unknown new phase, but only additional low-temperature XRD studies can answer this question. More important is the strong damping of the PAC spectra between 150 and 370 K. In analogy to the oxides, this reversible damping can be understood as dynamical hyperfine interaction, induced by the EC decay of the ^{111}In probes. However, it is still unknown why at very low temperatures, again electrons are available, as similarly observed in some oxides.

ACKNOWLEDGMENTS

The authors are indebted to D. Purschke for his help during the ^{111}In implantations and to C. Perez-Vicente for his helpful discussion on Rietveld analysis. This work was supported by the French-German PROCOPE Project No. 96068.

[1] A. Bartos, W. Bolse, K. P. Lieb, and M. Uhrmacher, Phys. Lett. A **130**, 177 (1988).

[2] Z. Inglot, D. Wiarda, K. P. Lieb, T. Wenzel, and M. Uhrmacher, J. Phys.: Condens. Matter **3**, 4569 (1991).

[3] D. Wiarda, T. Wenzel, M. Uhrmacher, and K. P. Lieb, J. Phys. Chem. Solids **53**, 1199 (1992).

[4] J. Shitu, D. Wiarda, T. Wenzel, M. Uhrmacher, K. P. Lieb, S. Bedi, and A. Bartos, Phys. Rev. B **46**, 7987 (1992).

[5] D. Lupascu, M. Uhrmacher, and K. P. Lieb, J. Phys.: Condens. Matter **6**, 10 445 (1994).

[6] A. Bartos, K. P. Lieb, A. F. Pasquevich, M. Uhrmacher, and ISOLDE Collaboration, Phys. Lett. A **157**, 513 (1991).

[7] A. Bartos, M. Uhrmacher, L. Ziegeler, and K. P. Lieb, J. Alloys Compd. **179**, 307 (1992).

[8] R. N. Attili, M. Uhrmacher, K. P. Lieb, L. Ziegeler, M. Mekata, and E. Schwarzmann, Phys. Rev. B **53**, 600 (1996).

[9] X. Korg *et al.* (unpublished).
[10] Z. Inglot, K. P. Lieb, M. Uhrmacher, T. Wenzel, and D. Wiarda, J. Phys.: Condens. Matter **3**, 3652 (1991).
[11] A. F. Pasquevich *et al.* (unpublished).
[12] A. F. Pasquevich, M. Uhrmacher, L. Ziegeler, and K. P. Lieb, Phys. Rev. B **48**, 10 052 (1993).
[13] G. A. Steigmann, H. H. Sutherland, and J. Goodyear, Acta Crystallogr. **19**, 967 (1965).
[14] R. Diehl, R. Nitsche, and C.-D. Carpentier, J. Appl. Crystallogr. **6**, 497 (1973).
[15] M. Uhrmacher, K. Pampus, F. J. Bergmeister, D. Purschke, and K. P. Lieb, Nucl. Instrum. Methods Phys. Res. B **9**, 234 (1985).
[16] M. Uhrmacher, M. Neubauer, W. Bolse, and K. P. Lieb, Nucl. Instrum. Methods Phys. Res. B **139**, 306 (1998).
[17] H. Frauenfelder and R. M. Steffen, in *Alpha, Beta and Gamma Ray Spectroscopy* (North-Holland, Amsterdam, 1965), Vol. 2, p. 997.
[18] G. Schatz and A. Weidinger, *Nukleare Festkörper Physik* (Teubner, Stuttgart, 1992).
[19] K. Alder, H. Albers-Schnberg, E. Heer, and T. B. Novey, Helv. Phys. Acta **26**, 761 (1953).
[20] J. Kajfosz (unpublished).
[21] A. Bartos, K. Schemmerling, Th. Wenzel, and M. Uhrmacher, Nucl. Instrum. Methods Phys. Res. A **330**, 132 (1993).
[22] M. Frank, F. Gubitz, W. Ittner, W. Kreische, A. Labahn, B. Röseler, and G. Weeske, Z. Naturforsch. Teil A **41A**, 104 (1985).
[23] G. Lanzendorfer, Ph.D. thesis, Erlangen, 1981.
[24] D. Lupascu, S. Habenicht, K. P. Lieb, M. Neubauer, M. Uhrmacher, T. Wentel, and ISOLDE Collaboration, Phys. Rev. B **54**, 871 (1996).
[25] S. Habenicht, D. Lupascu, M. Uhrmacher, L. Ziegeler, K. P. Lieb, and ISOLDE Collaboration, Z. Phys. B **101**, 187 (1996).
[26] M. Deicher, Hyperfine Interact. **79**, 681 (1993).
[27] M. Uhrmacher, L. Aldon, L. Ziegeler, F. Olivier-Fourcade, and J. C. Jumas (unpublished).
[28] M. Uhrmacher, V. V. Krishnamurthy, K. P. Lieb, A. Lopez Garcia, and M. Neubauer, Z. Phys. Chem. **206**, 249 (1998).
[29] D. B. Wiles and R. A. Young, J. Appl. Crystallogr. **28**, 366 (1995).
[30] P. G. Rustamov, P. K. Babaeva, and M. R. Allazov, Russ. J. Inorg. Chem. **24**, 1223 (1979).
[31] M. Womes, Ph.D. thesis, Saarbrücken, Germany, 1992.
[32] M. Womes, F. Py, M. L. Elidrissi Moubtassim, J. C. Jumas, J. Olivier-Fourcade, F. Aubertin, and U. Gonser, J. Phys. Chem. Solids **55**, 1323 (1994).
[33] M. Eibschutz, E. Hermon, and S. Shtrikman, Solid State Commun. **5**, 529 (1967).
[34] J. B. Goodenough and G. A. Fatseas, J. Solid State Chem. **41**, 1 (1982).
[35] D. Wiarda, M. Uhrmacher, A. Bartos, and K. P. Lieb, J. Phys.: Condens. Matter **5**, 4111 (1993).
[36] F. D. Feiock and W. R. Johnson, Phys. Rev. **187**, 39 (1969).
[37] R. M. Sternheimer, Phys. Rev. **130**, 1423 (1963).